Biogeotechnics 4 (2026) 100157

Contents lists available at ScienceDirect

Biogeotechnics

journal homepage: www.keaipublishing.com/en/journals/biogeotechnics/

Microbially induced carbonate precipitation for soil improvement: Insights from a meter-scale radial grouting trial

Guijie Sang[a,*], Rebecca J. Lunn[b], James M. Minto[b], Grainne El Mountassir[b]

[a] Department of Civil and Environmental Engineering, University of Liverpool, Liverpool, UK
[b] Department of Civil and Environmental Engineering, University of Strathclyde, Glasgow, UK

ARTICLE INFO

Keywords:
MICP
Biocementation
Radial flow
Large-scale
Two-phase grouting
$CaCO_3$ distribution

ABSTRACT

Despite the growing interest in microbially induced carbonate precipitation (MICP) for geotechnical applications, reports on meter-scale MICP trials for soil improvement remain limited, and controlling and predicting cementation efficiency on a large-scale is even more scarce. This study presented a meter-scale improvement of a poorly-graded sand (initial dry density: 1581 kg/m^3, porosity: 40 %) through MICP in a cylindrical cell (diameter: 1 m; thickness: 15 cm) using a radial flow injection strategy, which involves injecting fluids radially from a single well located at the center while maintaining a constant hydraulic head at the outer boundary. Nine cycles of a two-phase MICP treatment were applied: Phase 1- injection of 0.7 pore volumes (PVs) of bacterial solution and 1-L water pulse; Phase 2- injection of 1.4 PVs of 0.5 mol/L cementing solution in two stages (i) 0.7 PV injection two hours after the bacteria were injected, and (ii) a further 0.7 PV injection the following morning after an overnight static reaction period. We observed non-uniform $CaCO_3$ precipitations along the distance from the central well and over the depth, which was induced by the decreasing flux towards the outer boundary under the radial flow pattern, along with influences from layered soil packing and hydraulically induced flow channels. $CaCO_3$ precipitation with distance from the central well follows a symmetric Gaussian-type distribution, with sufficient cementation to retrieve full-length cores occurring near the midpoint between the central well and the outer boundary. The unconfined compressive strengths of the full-length cores were in the range of 1.2–6.8 MPa with $CaCO_3$ contents of 0.08–0.17. Our study suggests that cementation level under radial flow conditions is controllable on a large scale and highly dependent on the injection volume of both bacteria and rinsing water pulse. The study provides a solid baseline for predicting and controlling $CaCO_3$ distribution in large-scale MICP soil improvement using a two-phase radial injection approach.

1. Introduction

Microbially Induced Carbonate Precipitation (MICP) has emerged as a promising technique for soil improvement, offering a sustainable alternative to traditional soil stabilization methods (DeJong et al., 2006; Fu et al., 2023; Stocks-Fischer et al., 1999; Whiffin et al., 2007). This biogeochemical process involves the use of ureolytic bacteria, e.g. *Sporosarcina pasteurii*, to hydrolyze urea which produces carbonate ions, increases pH and results in the precipitation of calcium carbonate ($CaCO_3$) if calcium sources are available. The precipitated $CaCO_3$ acts as a binding agent, altering the properties of soil (or rock) such as increasing their strength and stiffness (Al Qabany & Soga, 2013; DeJong et al., 2006; Fu et al., 2023; Terzis & Laloui, 2018), and reducing permeability (El Mountassir et al., 2014; Hataf & Baharifard, 2020). As such, MICP has been demonstrated as a promising technique for many geotechnical engineering applications, including soil stabilisation (Al Qabany & Soga, 2013; Whiffin et al., 2007; Xiao et al., 2022), settlement reduction (Martinez & DeJong, 2009; Zamani et al., 2021), liquefaction mitigation (DeJong et al., 2022; Montoya & Dejong, 2013), and erosion resistance (Cheng et al., 2021; Gomez et al., 2015; Liu et al., 2021; Salifu et al., 2016; Xiao et al., 2022).

Although there is increasing interest in MICP for geotechnical applications, it remains predominantly confined to small scale laboratory tests, with only a few large-scale experiments having been completed (Gomez et al., 2015, 2017; Meng et al., 2021; Sang et al., 2024; Sharma et al., 2022; van Paassen et al., 2010; Xiao et al., 2022; Zeng et al., 2021; Terzis et al., 2020; van Paassen, 2011; Wu et al., 2020). These large-scale experiments have provided early insights into the practical

* Corresponding author.
E-mail address: g.sang@liverpool.ac.uk (G. Sang).

https://doi.org/10.1016/j.bgtech.2024.100157
Received 30 September 2024; Received in revised form 15 November 2024; Accepted 28 November 2024
Available online 9 December 2024
2949-9291/© 2025 The Authors. Publishing services by Elsevier B.V. on behalf of KeAi Communications Co. Ltd. This is an open access article under the CC BY license (http://creativecommons.org/licenses/by/4.0/).

challenges and outcomes of scaling up MICP from laboratory experiments to field applications, including large-scale bacterial cultivation under non-sterile conditions (Sang et al., 2024; Sharma et al., 2022; Zeng et al., 2021), in situ geophysical monitoring for non-destructive evaluation of treatment efficacy (Gomez et al., 2017; van Paassen et al., 2010), the potential to use native soil organisms in biostimulation approaches (Gomez et al., 2017), and the adoption of different hydraulic treatment methods such as surface percolation (Gomez et al., 2015; Xiao et al., 2022), or permeation grouting (Sang et al., 2023a; van Paassen, 2011), or the combination of both (Wu et al., 2020). Despite the promising results from the trials mentioned above, implementing MICP on a large scale continues to pose several challenges (Dejong et al., 2013; Filet et al., 2020; Fu et al., 2023), including large-scale cultivation of bacterial solution, uniform distribution of bacterial cultures and cementation solutions, as well as controlling the $CaCO_3$ precipitation process. Understanding the behavior of $CaCO_3$ precipitation under specific grouting strategies is crucial for optimizing the MICP process and ensuring its reliability in real-world applications. To date, studies focusing on evaluating $CaCO_3$ precipitation patterns on a large-scale using a single injection well based on a radial grouting strategy remain limited.

A previous study (Sang et al., 2023a) using MICP for improving medium-graded gravelly sand in a meter-scale round cell based on a radial flow grouting strategy. In this study, we will further investigate the improvement of poorly-graded sand on a meter scale using the same radial flow injection strategy but with a significantly reduced amount of bacterial and cementing solution (i.e. only 0.7 pore volumes). The aim of this study is to evaluate the extent of treatment under a radial injection two-phase treatment strategy, and to better understand the role of hydraulics on treatment efficacy and $CaCO_3$ precipitation distribution. Additionally, hydraulic properties are monitored throughout the treatment process, with overhead photos captured to visualize precipitation pattern and any flow channels induced during the treatment cycles. Treatment efficacy is evaluated based on the $CaCO_3$ distribution in the treated sand and the unconfined compressive strength test on the cores drilled from the treated sand. The study seeks to contribute to the understanding of large-scale MICP processes in poorly-graded sand using a single injection well, and sheds light on field MICP applications for soil improvement using multiple injection wells with scientifically designed grouting strategies.

2. Experiment methods

2.1. Materials

The sands used for the MICP experiment were poorly-graded according to ASTM D2487 - 17, with the median grain size (d_{50}) being 270 μm, and the grain sizes for which 60 %, 30 % and 10 % of the grains by mass are finer being 285 μm, 230 μm and 190 μm, respectively. The uniformity coefficient (d_{60}/d_{10}) and coefficient of curvature ($d_{30}^2/d_{60}/d_{10}$) were approximately 1.5 and 0.98, respectively.

Sporosarcina pasteurii (DSM No. 33) from glycerol stock stored in −80 °C was cultured into 2 L of autoclaved yeast extract media at a temperature of 30 °C on an orbital shaker at 115 r/min for 24 h. The yeast extract media contained 5.5 g/L yeast extract, 5 g/L sodium chloride, 0.4 g/L D-glucose and 0.4 g/L potassium phosphate dibasic, supplemented with filtered urea (20 g/L). The 2 L of cultured bacteria was then upscaled to grow 30 L bacterial solution in a 50 L fermentation tank (aeration rate: 9.2 L/min; temperature: 30 °C). The ureolytically active bacteria were harvested after 24 h. These procedures were repeated for a couple of times to obtain enough (~ 300 L after dilution to an OD_{600} of 1) bacterial solution and stored in the cold room for the MICP experiment. Before injection, the bacteria solution was diluted with water to achieve an optical density (OD_{600}) of 1 at a single wavelength of 600 nm.

2.2. Construction of the radial flow cell (RFC)

A radial flow cell (RFC), similar to that in a previous study (Sang et al., 2023a), was constructed to treat sand with MICP using a radial injection strategy. The schematic plot of the RFC is shown in Fig. 1, which consisted of an injection well located at the center and a constant hydraulic head at the outer boundary to replicate field conditions. The outer boundary was confined by a perforated plastic sheet (with evenly distributed 2 mm holes) and screened with a layer of 120 mol/L polyester silk mesh. The sand was added gradually and compacted by hand in the cell under water. The average initial dry density was estimated to be 1581 kg/m^3 based on the total mass of sand added, with an average porosity of 40.0 %. Thirteen piezometer tubes were buried within the sand during packing (Fig. 1A) to monitor pressure changes at different distances from the center. This design aimed to capture permeability at various locations in case permeability anisotropy occurred, and potentially allow for effluent sampling to confirm effective delivery of bacterial and cementing solution at these locations. However, among the thirteen piezometer tubes, only the one connected to the central injection well (mark by the red arrow in Fig. 1A & B) effectively recorded pressure changes over the nine MICP treatment cycles, while the other twelve became clogged with sands during initial permeability test. After the construction of the RFC and prior to MICP treatment, a fluorescein tracer pulse was injected via the central well to evaluate the flow pattern. Time-lapse ultraviolet (UV) fluorescence photos were taken overhead to confirm that flow in the cell follows the expected radial pattern (refer to Movie S1 in the Supplementary file). Unlike the previous study (Sang et al., 2023a), this study did not have a kaolinite layer on top of the sand layer to prevent bypass flow, as a radial flow pattern was successfully formed without inducing severe flow channels at the beginning. More importantly, the injection of bacterial and cementing solution was significantly reduced compared to the previous study to estimate the radial extent of treatment. This is further discussed in Section 2.3.

2.3. Injection strategy and permeability monitoring

The volume of bacteria injected in each treatment cycle was approximately 0.7 pore volumes (PVs) (~ 29 L) so that the radial extent of treatment could be evaluated. After injecting the bacterial solution at a flow rate of 2 L/min, 1 L of water was injected at a rate of 0.25 L/min to rinse the injection tubing and well and zone closest to the injection well, followed by a 2 h static period to allow bacterial attachment. The used of 1 L water will cover a radial extent of approximately 0.075 m in theory, which is sufficient to prevent well clogging within this range without overly impacting the overall cementation levels in the radial flow cell. Subsequently, a total 1.4 PV of 0.5 mol/L urea & $CaCl_2$ cementing solution was injected at a flow rate of 0.25 L/min, in two stages (i) 0.7 PV injection followed by overnight reaction period, and (ii) a further 0.7 PV injection in the following morning and left for 4 h before flushing another 1 L of water for well cleaning. These procedures constituted one treatment cycle, and they were repeated until the completion of nine treatment cycles over nine days. In total, in this study each cycle involved injection of 0.7 PVs and 1.4 PVs of 1.0 OD_{600} bacteria and 0.5 mol/L cementing solution respectively, as opposed to 2 PVs of bacteria and 2 PVs of cementing solution as used in the previous study by Sang et al. (2023a). The overhead photos of the RFC during the 9 cycles of MICP treatment were taken to visualize any flow channels formed and $CaCO_3$ precipitation on the top surface. After the MICP treatment, $CaCO_3$ precipitation at the top surface of the sand was visualized by a visible light source and an ultraviolet fluorescence source.

The permeability of the sand in the RFC was monitored before, during, and after MICP treatment cycles, based on pressure monitored at the injection port by the piezometer tube (connected to the injection port of the central well) shown in Fig. 1A. Specifically, prior to and after the MICP treatment, permeability was measured twice using water

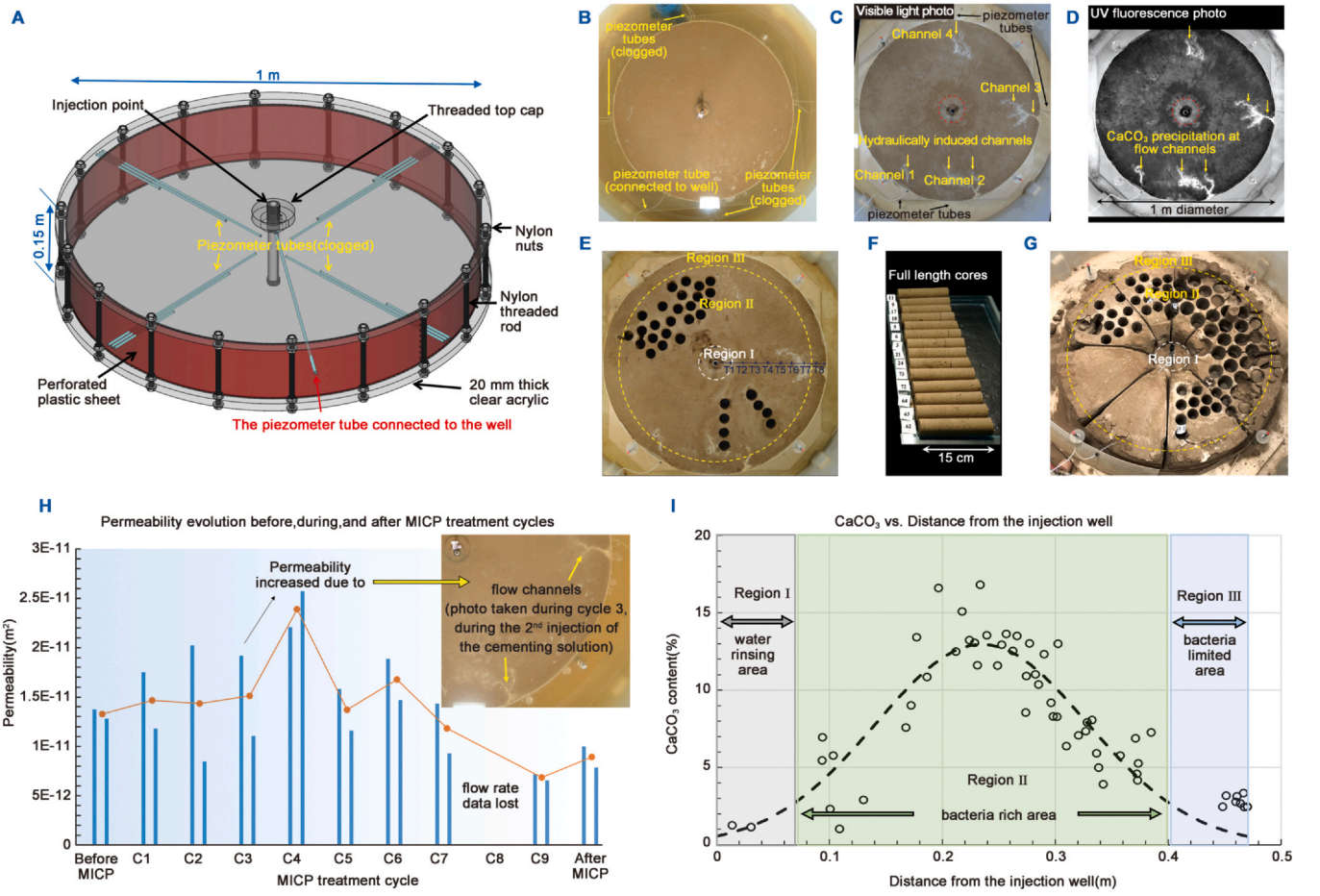

Fig. 1. (**A**) Schematic of the RFC; (**B**) An overhead photo taken during the injection of bacterial solution in the 1st treatment cycle; (**C–D**) Overhead photo of the RFC after the cover was removed showing $CaCO_3$ precipitation (white precipitates). The two photos were taken by (C) visible light source, and (D) ultraviolet fluorescence source; (**E**) Overhead photo of the treated sand after cutting some 36 mm diameter cores, showing three regions: Region I with poor cementation and lacking intact cores, Region II with good cementation producing full-length (0.15 m) cores, and Region III with insufficient cementation for full length cores. (**F**) Full-length cores drilled from the RFC within Region II. (**G**) The sand left after coring and cutting, with loose sand removed from Region I, and coring holes remaining in Region II. (**H**) Changes in permeability before, during and after MICP cycles. The permeability for each MICP cycle was measured during the 1st injection of the cementing solution (orange dot represents the average value at each cycle). (**I**) $CaCO_3$ content plotted against the distance from the injection well. Scattered circles represent measured data, while dashed line was fitted based on the Gaussian equation (refer to the Appendix in the Supplementary file for the fitting parameters and the goodness of fitting).

injection at the rate of ~ 0.25 L/min. During MICP treatment cycles, permeability was measured during the injection of 1st cementing solution (rate: 0.25 L/min), which was calculated twice based on the pressure difference between (1) the initial static pre-injection pressure and the average static pressure during injection, (2) the average static pressure during injection and the post-injection static pressure. Note that the pressure evolution was also monitored during the injection of the bacterial solution. However, in this study, we only calculated the permeability based on the injection of water and the 0.5 mol/L cementing solution, due to their similar viscosity and injection rate (~ 0.25 min/L).

2.4. Post-treatment analysis

After MICP treatment, the RFC was flushed with 2 PVs of water to remove residual chemicals and bacteria. After the top cover was removed, acoustic testing on 8 spots along the distance from the central well was performed using a stainless-steel spoon to roughly evaluate the treatment efficacy in the RFC. Subsequently, cores > 70 were drilled using a water-cooled concrete coring bit with the coring frame and pad sitting on top of the RFC (coring locations are labelled in Fig. S1 in the Supplementary file). These intact cores were subjected to a series of geotechnical tests and microstructural analyses, such as unconfined compressive strength and $CaCO_3$ content tests, 2-dimensional X-ray radiography, and 3-dimensional X-ray micro-computed tomography (CT). Finally, the treated sand in the RFC was saw-cut into 8 pieces along the black dashed lines in Supplementary Fig. S1 to further evaluate the treatment effectiveness (e.g. sampling of small pieces for $CaCO_3$ content test).

2.4.1. Unconfined compressive strength (UCS)

The UCS test was conducted for twenty-eight core samples (length to diameter ratio: 2) drilled within distances between 0.17 m to 0.31 m from the center. The core samples were firstly oven-dried at 60 °C until no further mass decrease was observed. Prior to the UCS test, the top and bottom surfaces of the core samples were polished with a sandpaper, and then capped with either gypsum plaster (Crystacast, compressive strength of 55.2 MPa) in accordance with the standard method ASTM C617/C617M-15. The caps were applied to provide smooth flat ends to the samples in order to minimize the effect of stress concentrations which can occur when uneven surfaces are loaded. A displacement rate of 0.2 mm/min was applied during the UCS test.

2.4.2. $CaCO_3$ contents

The $CaCO_3$ content was determined using the acid washing method. For the thirty-nine UCS tested core specimens, ~ 30–60 g of each sample were collected from near the failure plane. Additionally, we also collected small samples (5–10 g) from twenty-six other locations (A–Z in Supplementary Fig. S1) in the RFC. Some locations (H, I, J, K, N, O) were also sampled at different depths (i.e. 0.025, 0.05, 0.075, 0.1, 0.125, and 0.15 m) to assess the cementation with depth. The collected samples were fully digested in flasks using ~ 1.2 mol/L hydrochloric acid (HCl). Then, all the solution and insoluble solids were washed with deionized water. The washed fluids were filtered through a filter paper powered by a vacuum pump. The washing process aimed to remove calcium chloride and excess hydrochloric acid. The $CaCO_3$ content was calculated as

$$CaCO_3(\%) = \frac{W_1 - (W_2 + \Delta w_f)}{W_1} \times 100\%$$

where W_1 is the dried mass of the bio-cemented sand before acid washing; W_2 is the dried mass of solids remained in the flasks after acid washing, excluding a small amount of insoluble solids (e.g. fine grains) that were washed out and attached to the filter paper; Δw_f is the mass change of the dried filter paper due to the washed out insoluble fine grains. The sum of $(W_2 + \Delta w_f)$ represents the dried mass of sand after removing $CaCO_3$.

2.4.3. X-ray radiography (2D) and computed tomography (3D)

14 core samples were subjected to 2D radiography at both 0° and 90°. One of the core samples (#9) was cut and scanned with 3D X-ray micro computed tomography (CT). The scanning parameters were 150 kV, 166 μA, 708 ms exposure time, with a voxel size of 90 μm. Single shading correction was used for all samples, with each image being the average of 16 frames.

3. Results

3.1. Permeability evolution

The initial permeability of the sand in the RFC was 1.3×10^{-11} m^2, remaining virtually unchanged during the first three treatment cycles. However, it increased to 2.4×10^{-11} m^2, as measured during the 4th MICP treatment cycles (Fig. 1H). This slight increase in permeability was likely caused by hydraulically induced flow channels formed in cycle 3 (Fig. 1H inset; also refer to Supplementary Movie S2 for fluid leakage along flow channel 2 during the second injection of cementing solution in MICP Cycle 3). Then, the permeability reduced to a final value of 8.9×10^{-12} m^2 after five additional treatment cycles due to the precipitation of $CaCO_3$. Note that the permeability from cycle 9 (Fig. 1H), as measured during the injection of the 1st cementing solution, exhibited slightly lower value than the final permeability, measured by deionized water after MICP. This may be due to the rapid reaction between the cementing solution and bacterial solution during the injection of the cementing solution in cycles 9, which increased the viscosity of the mixed solution. This reaction was absent during the final permeability measurement using deionized water. However, there was no noticeable difference between the initial permeability (measured with deionized water) and the permeability measured in cycle 1–3. The maximum pressure at any point during treatment was only 6.8 kPa, equivalent to a pressure head of 0.7 m of water. This indicates that the sand remains free-draining throughout the treatment cycles without generating much back pressure, and confirms that low pressure equipment can be used for field-scale MICP treatment.

$CaCO_3$ precipitation at the top surface of the RFC after 9 cycles of MICP treatment can be visualized by visible light and UV fluorescence photos as shown in Fig. 1(C–D), respectively. Overall, the formation of $CaCO_3$ in the RFC is observed as being radially symmetric, following the radial injection of bacteria/cementing solution. Massive $CaCO_3$ precipitations occurred at hydraulically induced channels (white precipitates in the RFC in Fig. 1(C–D), which were absent prior to the MICP treatment as shown in Fig. 1B. All the channels (1–4) were located on the top sand surface near the buried piezometer tubes, as marked in Fig. 1C (also refer to Supplementary Movie S2 for fluid leakage along flow channel 2). These channels were likely induced by hydraulic erosion near the buried piezometer tubes (soft silicones), where compression may have caused subsidence and, hence, a slight gap and bypass flow between the top cover and the sand, leading to the formation of eroded channels. During the later treatment cycles (5–9th), $CaCO_3$ precipitation gradually filled the channels, resulting in a decrease in the overall permeability of the RFC.

Notably, within the water rinsing region (a radial distance of approximately 0.075 m), there was a relatively well cemented thin layer (~ 1–2 cm thick) as indicated by the white precipitates delineated by the red dashed circle in Fig. 1H and C. Below this thin layer (~ 1 cm), the sand was not well cemented, which will be detailed in the next section. This well-cemented thin layer near the central well was possibly formed due to less preferential flow at this location, which was less affected by the rinsing water but allowed the diffusion of bacteria (or their mobility) and cementing solutions during MICP treatment cycles.

3.2. Examination of overall treatment efficacy

The RFC was divided into three regions (i.e. Regions I–III as shown in Fig. 1E, G & I), depending on the cementation level from the acoustic test (see Movie S3 in the Supplementary file), coring and cutting results (Fig. 1E & G), and $CaCO_3$ content relative to the distance from the central well (Fig. 1I). The acoustic test using a stainless-steel spoon on eight spots on the top surface of the RFC (see Supplementary Movie S3), revealed that the sand exhibited a muffled and soft sound at spot T1 (radial distance: 0.075 m). Another observation is that within Region I, the sands were loose and easy to excavate during the final cutting process, as shown in Fig. 1G. This is due to the poor cementation, with only < 3 % $CaCO_3$ precipitation (Fig. 1I) within a radial distance of 0.075 m (Region I) from the injection point. The low $CaCO_3$ in Region I can be explained by the injection of 1 L of water twice – once after the bacterial solution was injected in a treatment cycle, and again before the next treatment cycle, which acts to (1) drain pore water bacteria within the radial range of 0.075 m, and (2) detach bacteria within this range. This water injection had a radial extent of approximately 0.075 m. The use of water with low ionic strength to facilitate bacterial detachment (Choi et al., 2017; Sang et al., 2023b) was also adopted by Sang et al. (2023a) to flush the near-well area and prevent well-clogging. Additionally, the injection rate of bacteria solution was 2 L/min, resulting in a Darcy velocity of 1273 cm/h at the injection point. The fluid velocity during radial flow is inversely proportional to the distance from the central injection well. Hence, hydrodynamic forces are much higher in the central injection zone (Region I), preventing bacterial attachment (El Mountassir et al., 2014; Sang et al., 2023a) and thus $CaCO_3$ precipitation.

As the radial distance from the central well increased from 0.075 m to 0.235 m (within Region II), $CaCO_3$ content rose from 3% (based on the Gaussian fitting curve in Fig. 1I, details on the Gaussian Equation and the fitting results can be found in the Appendix in the Supplementary file) to a maximum of 17 %. The increasing level of cementation was also demonstrated by the progressively sharper sounds from T1 to T4 emitted during acoustic testing using a stainless-steel spoon (refer to Supplementary Movie S3). The increasing cementation from radial distance of 0.075 m to 0.235 m was likely induced by an increasing level of bacterial concentration due to (1) a decreasing water flux (flow rate per unit area, defined in Supplementary Fig. S2) and a consequent reduction in the water rinsing effect, (2) a decreasing flow velocity, which reduced hydrodynamic forces under the radial flow

regime and promoted higher bacterial attachment. Spots T4, T5, T6, and T7 at radial distances of 0.22 m, 0.27 m, 0.32 m, 0.37 m, maintained excellent cementation within Region II, as demonstrated by a sharp, resonant, rock-like sound (Movie S3) and the majority of full-length cores drilled from this region with the distances between 0.17 m and 0.31 m from the well. The area of Region II accounted for approximately 70 % of the total RFC area, which is consistent with the injection of 0.7 PVs of bacterial solution (i.e. 70 % of the total pore volume), as well as the injection of 0.7 PV of cementing solution twice. The $CaCO_3$ content peaked at the radial distance of 0.235 m and then started to decline due to the decreasing flux of bacteria.

With further increasing distance from the central well, from 0.235 m to 0.4 m, the decreasing flux of 0.7 PVs of bacterial and cementing solutions caused the drops in $CaCO_3$ content. At spot T8 (radial distance: 0.42 m) as shown in Fig. 1E, the cementation level (i.e. $CaCO_3$ content) declined to approximately 2 % (Fig. 1I), causing the less sharp and less resonant sound during the acoustic test (Movie S3), and the lack of full-length cores drilled from this area (Fig. 1G). In Region III near the boundary beyond the outer yellow dashed circle (radial distance: 0.4–0.47 m from the central well), the sand was less effectively cemented due to (i) limited volumes of bacterial solution (i.e. only 0.7 PVs of bacterial solution was injected for each treatment cycle), which did not fill the entire pore volume within the RFC, and (ii) the reduction in the flux of bacteria and cementing solution with increasing distance from the central injection well, due to the radial flow regime. Overall, high levels of cementation ($CaCO_3$ contents higher than 5%) were observed in the RFC within a 0.1–0.37 m radial distance from the central injection well, allowing full-length cores to be drilled at 0.17–0.31 m radial distance.

3.3. Unconfined compressive strength (UCS) results

The UCS of the core samples, drilled from the well-cemented zone within a 0.17–0.31 m radial distance, ranged from 1.2 to 6.8 MPa, with their $CaCO_3$ contents ranging from 0.08 to 0.17. The UCS curves with compressive stress plotted against axial strain is shown in Supplementary Fig. S3 a. Most cores exhibited brittle failure, characterized by a sudden drop in stress after reaching the peak value. These samples displayed shear or tensile failure modes (Supplementary Fig. S3 b). Fig. 2A shows the UCS values and their $CaCO_3$ contents, plotted alongside other published meter-scale MICP trials by van Paassen et al. (2010) and Wu et al. (2020) which also used poorly-graded sand, and by Sang et al. (2023a) which used medium-graded gravelly sand. Among these large-scale MICP trials, the UCS values for the cores in this study are notably stronger than the poor-graded sand by van Paassen et al. (2010) and Wu et al. (2020), but slightly weaker than the medium-graded sand by Sang et al. (2023a) for a given $CaCO_3$ content.

Fig. 2B–H show the 2D radiography (taken at 0° and 90°) and 3D X-ray CT scans of a full-length 15 cm core drilled across the entire depth of the RFC. The 2D radiography exhibited three layers (Fig. 2B) in a full-length core (#9), which correspond to the 3 layers in which the sand was compacted, with the bottom layer (layer 3) showing the noticeably highest density (Fig. 2C), and the middle layer (layer 2) showing the least density. The 2D radiographs of other samples in Supplementary Fig. S4 also showed different layers of sand, with similarly higher density at the bottom of specimens for most full-length cores. The higher density near the bottom of specimens can be attributed to either greater initial compaction, as evidenced by the three distinct layers shown in Fig. 2B, or increased calcium carbonate precipitation, as shown in Fig. 2G, where the upper section (< 0.075 m) generally exhibits lower $CaCO_3$ content compared to the lower section (0.075–0.15 m). A higher initial packing density near the bottom could provide a more surface area per unit volume for bacterial attachment, thereby enhancing $CaCO_3$ precipitation. Additionally, the gravitational effect may have contributed to increased $CaCO_3$ precipitation by concentrating bacterial and cementing solutions toward the bottom. However, this gravitational effect alone would likely cause a gradual increase in $CaCO_3$ precipitation toward the bottom rather than forming three distinct layers. Therefore, the higher $CaCO_3$ near the bottom is likely because of initial packing and, possibly, gravitational influence.

A similar pattern is observed in Supplementary Fig. S5 for locations H, I, J, K, N, and O (see Supplementary Fig. S1 for these locations), where $CaCO_3$ content is higher near the bottom (depths of 0.125–0.15 m) and lower in the middle (depths of 0.05–0.1 m). Near the surface (depth of 0.025 m, Supplementary Fig. S5), samples from locations H, I, K, N, and O display higher $CaCO_3$ content than in the middle range (depths of 0.05 and 0.075 m). This is likely due to preferential bypass flow near the surface, particularly at locations K, N, and O, where flow channels were formed, as seen in Supplementary Fig. S1 and Fig. 1C& D, resulting in higher flux near these regions.

Fig. 2D shows the 3D X-ray CT image for the sample cut from the lower part of the full-length core #9, which has notably more macro pores and a lower sample density in the upper part of the scanned core (Fig. 2E). Note that the upper part of the core sample #9 corresponds to the middle depth in the radial flow cell (i.e. layer 2 in Fig. 2B). During UCS testing, failure occurred in the upper part of the core (Fig. 2F), where lower density, as evidenced in Fig. 2(C–E), and lower $CaCO_3$ content (0.146, compared to the bottom $CaCO_3$ of 0.182) were observed. Note that apart from the effect of the precipitated $CaCO_3$ content (Fig. 2A), the strength of the bio-cemented cores is also known to be controlled by grain size, shape and distribution (Song et al., 2022; Terzis & Laloui, 2018; Xiao et al., 2021, 2019a, 2019b), the presence of fines (Ma et al., 2021, 2022), the uniformity of $CaCO_3$ (Zhang et al., 2023), the patterns of $CaCO_3$ precipitation (e.g. bridging, pore filling, surface coating, etc.) (Lai et al., 2024; Wu et al., 2023).

Fig. 2H shows the secondary electron image of one of the core samples, demonstrating that the precipitated calcium carbonates were calcite crystals encapsulating bacterial cells. Additional secondary electron images and the Energy-dispersive X-ray spectroscopy (EDS) analyses are available in Supplementary Fig. S6, which also exhibit calcite crystals. As noted by Chen et al. (2022a, 2022b), precipitated $CaCO_3$ initially assembles as amorphous calcium carbonate in an orderly manner and gradually transforms into calcite crystals, similar to the biologically induced calcium carbonate precipitation observed in mollusk shell (Falini et al., 1996). Controlling effective cementation by bio-cement (calcite, in this study) is crucial for achieving higher soil improvement efficiency (Chen et al., 2022b), though it remains less thoroughly investigated in large-scale MICP trials.

4. Discussion

El Mountassir et al. (2018) outlined some technical challenges of large-scale MICP soil improvement, including the prevention of clogging near injection wells and the achievement of a relatively uniform cementation in the target treatment zone. Both this study and a previous large-scale trial by Sang et al. (2023a) have highlighted that using water pulses, in combination with radial flow, can effectively rinse the near well area, preventing bacterial attachment and subsequent well clogging through $CaCO_3$ precipitation.

Under a radial injection scheme, which is one of the most common grouting methods in practical engineering, non-uniformity in $CaCO_3$ distribution is technically inevitable due to the decreasing flux towards the outer radial direction. In this study, bacteria/cementing solutions were injected through a single central well, forming a radial flow pattern as expected (Movie S1). The $CaCO_3$ precipitation along the distance from the central well followed a Gaussian-type distribution, with the peak $CaCO_3$ content occurring midway between the outer boundary and the central injection well (i.e. at a radial distance of 0.235 m), and $CaCO_3$ contents of over 5% were achieved within the radial distance of 0.1–0.37 m. In the field, it is recommended that ‘nested’ injection strategies are used, whereby a grid of injection wells is deployed in

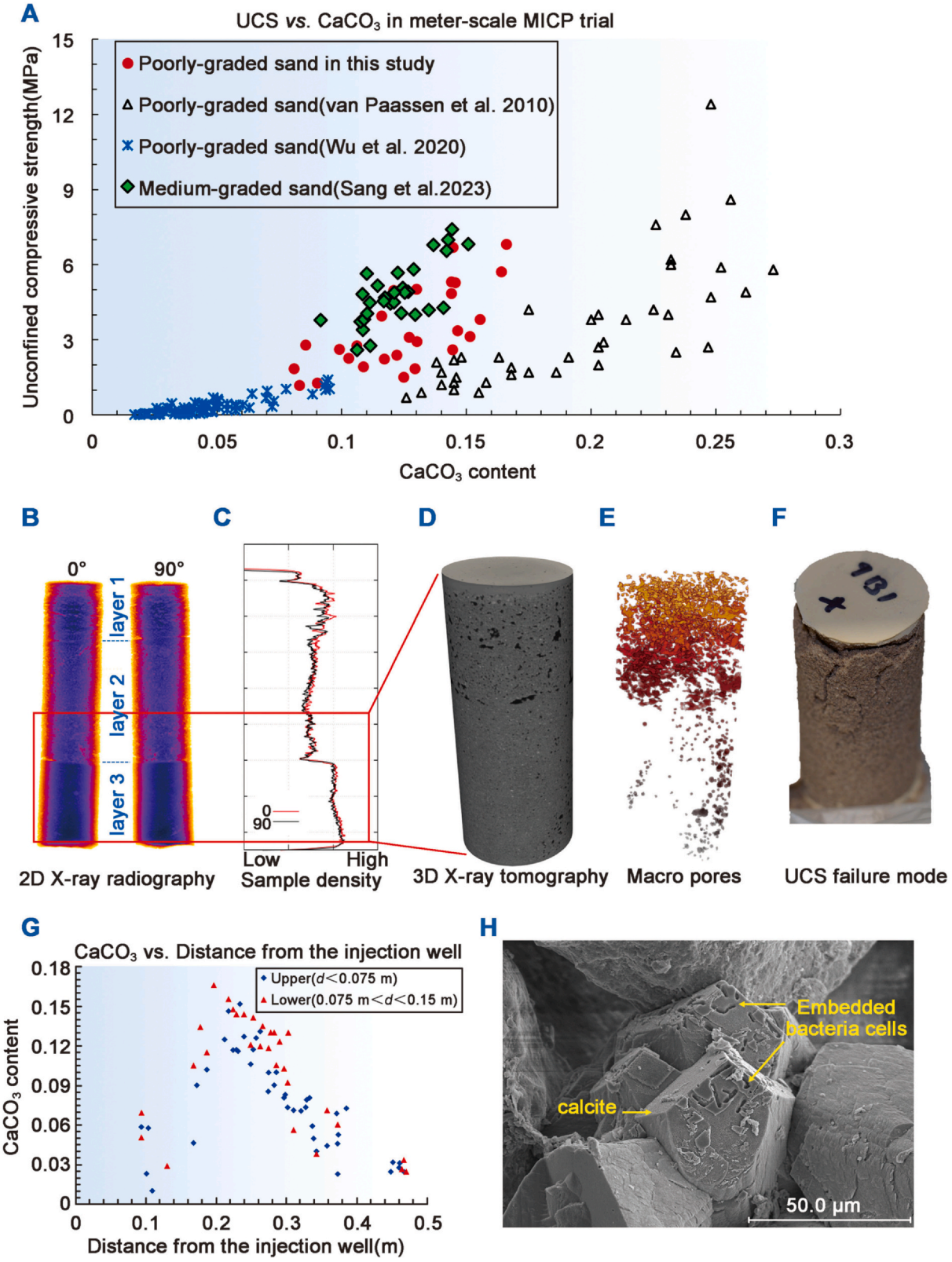

Fig. 2. (**A**) UCS plotted against $CaCO_3$ content in comparison with other studies on meter-scale MICP trials. van Paassen et al. (2010) and Wu et al. (2020) used poorly-graded sand (uniformity coefficient ~ 1.5–1.6), while Sang et al. (2023a) used medium-graded gravelly sand.(**B**) 2D X-ray radiography of a full-length core drilled across the depth of the RFC (length: 15 cm); (**C**) Corresponding density profile with depth obtained from the 2D X-ray radiography; (**D**) A 3D X-ray CT scan of the 2:1 core capped and prepared for UCS testing; (**E**) Segmented macro pores based on the 3D X-CT scan; (**F**) Failure mode for the 3D X-CT scanned sample. (**G**) $CaCO_3$ content averaged along depth, plotted against the distance from the injection well. Blue squares represent the samples from the upper section (depth < 0.075 m), while red triangles represent the samples from the lower section (0.075 < depth < 0.15 m). Note that the two samples near the injection well (location Z in Supplementary Fig. S1) were collected from a mixture of loose sands in that region. Since their depth is unknown, these two samples were not plotted in Fig. 2G; however, they are presented in Fig. 1I. (**H**) Secondary electron images of the sample showing calcite crystals with embedded rod-like bacterial cells.

Phase I, followed by Phase II injection at new wells located in-between the wells in Phase I. This "nested" two-phase injection strategy was numerically simulated by Minto et al. (2019) and a relatively uniform distribution of $CaCO_3$ (60–120 kg/m^3) was predicted within a 2-dimensional 18 × 18 m^2 domain.

In this study, non-uniform formations of $CaCO_3$ were also observed due to variations in sand packing and hydraulic channeling. For example, Supplementary Fig. S5 shows the non-uniform $CaCO_3$ content with respect to depths at five different locations in the RFC, all exhibiting a better cementation near the bottom of the cell. As mentioned, this was likely induced by one or more of the following factors (1) sand packing in three layers, which led to a higher initial packing density near the bottom, as evidenced by the 2D radiography (Fig. 2B & C and Supplementary Fig. S4); (2) the increased surface area per unit volume in the densely packed areas, which may have allowed for more bacterial attachment; and (3) the potential accumulation of bacterial/cementing solution near the bottom due to gravitational effects. Additionally, clear $CaCO_3$ rich pathways were observed to form in hydraulically induced flow channels (Fig. 1C & D). Despite the presence of these flow channels during the treatment cycles, the permeability of the RFC didn't increase significantly (Fig. 1H), and the flow in the cell remained largely radial without the loss of too many bacteria/cementing solutions into the channels. As a result, approximately 70 % areas in the RFC (within the distance range of 0.07–0.40 cm) were well cemented as a result of 0.7 PVs of bacterial solution being injected in each cycle. Furthermore, the formation of hydraulically induced channels in the field is unlikely, as sufficient overburden pressure effectively prevents their development.

Our study demonstrates that the cementation level (i.e. $CaCO_3$ content) within the radial flow cell, in relation to the distance from the central injection well, follows a Gaussian distribution, as shown in Fig. 1I. This distribution is likely a result of the combined effects of the injected bacterial solution, rinsing water, and cementing solution in each treatment cycle, which influence the transport and retention of bacteria within the sand in the radial flow cell. It is expected that a higher volume of rinsing water injection would result in a rightward shift of the Gaussian's mean value (i.e. the distance at which peak $CaCO_3$ content occurs), while a higher volume of bacterial solution (and cementing solution) injection would increase the overall cementation level (i.e. an upward shift of the distribution curve). However, further experimental evidence is still needed to validate this hypothesis, and the effect of the water-to-bacterial solution ratio on the uniformity of $CaCO_3$ precipitation remains an open question for future investigation.

5. Conclusion

This study demonstrates successful meter-scale improvement of poorly-graded sands using MICP, with bacteria and cementing solutions injected via a central injection well designed to replicate in situ soil improvement in the field using MICP. The following key conclusions can be drawn:

During the nine treatment cycles, the permeability of the RFC increased slightly from 1.3×10^{-11} m^2 to 2.4×10^{-11} m^2, due to channel formation during injection, then declined to 8.9×10^{-12} m^2 as precipitation increased. This means that the sand remained permeable and free-draining throughout the entire MICP treatment.

The $CaCO_3$ content achieved after treatment follows a Gaussian-type distribution with distance from the central well, exhibiting a symmetric profile with the peak $CaCO_3$ content of approximately 13% (fitted value) occurring at a radial distance of 0.235 m (i.e. the midpoint between the central well and the boundary). This distribution closely corresponds to the radial extent of water rinsing and the volume of bacterial/cementing solution injected in each cycle (0.7 PVs in this study).

Full-length cores were successfully drilled within a 0.17–0.31 m radial distance from the injection point, with UCS values of 1.2–6.8 MPa corresponding to $CaCO_3$ contents of 0.08–0.17. The UCS values of the tested cores in this study exceed those obtained by previous researchers using poorly-graded sand when plotted against $CaCO_3$ contents for samples.

The flow in the test cell followed a radial pattern with a decreasing flux towards the outer boundary. As expected, this resulted in a decreasing $CaCO_3$ content with increasing distance from the central well in areas away from the water rinsing region. The layered packing, as evidenced by the 2D radiography and 3D X-CT scans, also caused non-uniform $CaCO_3$ precipitation over depth due to variations in the packing densities of the sand between layers. Despite the presence of layers and hydraulically induced flow channels, $CaCO_3$ precipitation in the cell was approximately radially symmetric with sufficient cementation achieved after nine treatment cycles to achieve intact, strong cores. Our results confirm that bacterial biomineralization is a viable alternative to cement for earth infrastructure applications.

CRediT authorship contribution statement

Guijie Sang: Writing – review & editing, Writing – original draft, Methodology, Formal analysis, Data curation, Conceptualization. **Rebecca J. Lunn:** Writing – review & editing, Supervision, Project administration, Investigation, Funding acquisition. **James M. Minto:** Writing – review & editing, Visualization, Methodology, Formal analysis, Data curation, Conceptualization. **Grainne El Mountassir:** Writing – review & editing, Visualization, Supervision, Methodology, Investigation, Conceptualization.

Data Availability

All data underpinning this publication are openly available from the University of Liverpool's Research Data Catalogue at 10.17638/datacat.liverpool.ac.uk/2863.

Declaration of Competing Interest

The authors declare that they have no known competing financial interests or personal relationships that could have appeared to influence the work reported in this paper.

Acknowledgements

This research was funded by the BAM Nuttall/Royal Academy of Engineering Research Chair in Biomineral Technologies for Ground Engineering. The contribution of El Mountassir was supported by a UKRI Future Leaders Fellowship (MR/V025376/1). We thank Jason Eriksen from the Department of Civil and Environmental Engineering for collecting the SEM images.

Appendix A. Supporting information

Supplementary data associated with this article can be found in the online version at doi:10.1016/j.bgtech.2024.100157.

References

Al Qabany, A., & Soga, K. (2013). Effect of chemical treatment used in MICP on engineering properties of cemented soils. *Géotechnique, 63*, 331–339. https://doi.org/10.1680/geot.SIP13.P.022

Chen, Y., Wang, S., Tong, X., & Kang, X. (2022a). Crystal transformation and self-assembly theory of microbially induced calcium carbonate precipitation. *Applied Microbiology and Biotechnology, 106*, 3555–3569. https://doi.org/10.1007/S00253-022-11938-7/FIGURES/10

Chen, Y., Wang, S., Tong, X., & Kang, X. (2022b). Towards the sustainable fine control of microbially induced calcium carbonate precipitation. *Journal of Cleaner Production, 377*, Article 134395. https://doi.org/10.1016/J.JCLEPRO.2022.134395

Cheng, Y. J., Tang, C. S., Pan, X. H., Liu, B., Xie, Y. H., Cheng, Q., & Shi, B. (2021). Application of microbial induced carbonate precipitation for loess surface erosion control. *Engineering Geology, 294*, Article 106387. https://doi.org/10.1016/J.ENGGEO.2021.106387

Choi, N.-C., Choi, J.-W., Kwon, K.-S., Lee, S.-G., & Lee, S. (2017). Quantifying bacterial attachment and detachment using leaching solutions of various ionic strengths after bacterial pulse. *AMB Express, 7*(1), 1–9. https://doi.org/10.1186/S13568-017-0340-2

DeJong, J. T., Fritzges, M. B., & Nüsslein, K. (2006). Microbially induced cementation to control sand response to undrained shear. *Journal of Geotechnical and Geoenvironmental Engineering, 132*, 1381–1392. https://doi.org/10.1061/(ASCE)1090-0241(2006)132:11(1381)

DeJong, J. T., Gomez, M. G., San Pablo, A. C., Graddy, C. M. R., Nelson, D. C., Lee, M., Ziotopoulou, K., El Kortbawi, M., Montoya, B., Kwon, T. H., 2022. State of the art: MICP soil improvement and its application to liquefaction hazard mitigation. In *Proceedings of the 20th ICSMGE-state of the art and invited lectures*.

Dejong, J.T., Soga, K., Kavazanjian, E., Burns, S., Van Paassen, L.A., Al Qabany, A., Aydilek, A., Bang, S.S., Burbank, M., Caslake, L.F., Chen, C.Y., Cheng, X., Chu, J., Ciurli, S., Esnault-Filet, A., Fauriel, S., Hamdan, N., Hata, T., Inagaki, Y., Weaver, T. (2013). Biogeochemical processes and geotechnical applications: Progress, opportunities and challenges. In *Proceedings of the bio- and chemo- mechanical processes in geotechnical engineering - Geotechnique symposium in print* (vol. *2013*, pp. 143–157). https://doi.org/10.1680/bcmpge.60531.014.

El Mountassir, G., Lunn, R. J., Moir, H., & MacLachlan, E. (2014). Hydrodynamic coupling in microbially mediated fracture mineralization: Formation of self-organized groundwater flow channels. *Water Resources Research, 50*, 1–16. https://doi.org/10.1002/2013WR013578

El Mountassir, G., Minto, J. M., van Paassen, L. A., Salifu, E., & Lunn, R. J. (2018). Applications of microbial processes in geotechnical engineering. *Advances in Applied Microbiology, 104*, 39–91. https://doi.org/10.1016/BS.AAMBS.2018.05.001

Falini, G., Albeck, S., Weiner, S., & Addadi, L. (1996). Control of aragonite or calcite polymorphism by mollusk shell macromolecules. *Science, 271*(1979), 67–69. https://doi.org/10.1126/SCIENCE.271.5245.67

Filet, A. E., Gutjahr, I., Garandet, A., Viglino, A., Béguin, R., Monier, J.-M., Oxarango, L., Emeriault, F., & Perthuisot, S. C. (2020). BOREAL, Bio-reinforcement of embankments by biocalcification. *E3S web of conferences* (pp. 5001). EDP Sciences.

Fu, T., Saracho, A. C., & Haigh, S. K. (2023). Microbially induced carbonate precipitation (MICP) for soil strengthening: A comprehensive review. *Biogeotechnics*Article 100002.

Gomez, M. G., Anderson, C. M., Graddy, C. M. R., DeJong, J. T., Nelson, D. C., & Ginn, T. R. (2017). Large-scale comparison of bioaugmentation and biostimulation approaches for biocementation of sands. *Journal of Geotechnical and Geoenvironmental Engineering, 143*, Article 04016124. https://doi.org/10.1061/(ASCE)GT.1943-5606.0001640

Gomez, M. G., Martinez, B. C., DeJong, J. T., Hunt, C. E., deVlaming, L. A., Major, D. W., & Dworatzek, S. M. (2015). Field-scale bio-cementation tests to improve sands. *Proceedings of the Institution of Civil Engineers - Ground Improvement, 168*, 206–216. https://doi.org/10.1680/grim.13.00052

Hataf, N., & Baharifard, A. (2020). Reducing soil permeability using microbial induced carbonate precipitation (MICP) method: A case study of shiraz landfill soil. *Geomicrobiology Journal, 37*, 147–158.

Lai, H. J., Ding, X. Z., Cui, M. J., Zheng, J. J., Chu, J., & Chen, Z. B. (2024). Factors affecting the effectiveness of biocementation of soil. *Biogeotechnics*Article 100087.

Liu, B., Xie, Y. H., Tang, C. S., Pan, X. H., Jiang, N. J., Singh, D. N., Cheng, Y. J., & Shi, B. (2021). Bio-mediated method for improving surface erosion resistance of clayey soils. *Engineering Geology, 293*, Article 106295. https://doi.org/10.1016/J.ENGGEO.2021.106295

Ma, G., He, X., Jiang, X., Liu, H., Chu, J., & Xiao, Y. (2021). Strength and permeability of bentonite-assisted biocemented coarse sand. *Canadian Geotechnical Journal, 58*, 969–981. https://doi.org/10.1139/CGJ-2020-0045/ASSET/IMAGES/CGJ-2020-0045EQ7.GIF

Ma, G., Xiao, Y., He, X., Li, J., Chu, J., & Liu, H. (2022). Kaolin-nucleation-based bio-treated calcareous sand through unsaturated percolation method. *Acta Geotechnica, 17*, 3181–3193. https://doi.org/10.1007/S11440-022-01459-Y/FIGURES/12

Martinez, B.C., & DeJong, J.T. (2009). Bio-mediated soil improvement: Load transfer mechanisms at the micro- and macro- scales, 242–251. https://doi.org/10.1061/41025(338)26.

Meng, H., Gao, Y., He, J., Qi, Y., & Hang, L. (2021). Microbially induced carbonate precipitation for wind erosion control of desert soil: Field-scale tests. *Geoderma, 383*, Article 114723.

Minto, J. M., Lunn, R. J., & El Mountassir, G. (2019). Development of a reactive transport model for field-scale simulation of microbially induced carbonate precipitation. *Water Resources Research, 55*, 7229–7245.

Montoya, B. M., & Dejong, J. T. (2013). Healing of biologically induced cemented sands. *Geotechnique Letters, 3*, 147–151. https://doi.org/10.1680/GEOLETT.13.00044/ASSET/IMAGES/SMALL/GEOLETT3-147-F3.GIF

Salifu, E., MacLachlan, E., Iyer, K. R., Knapp, C. W., & Tarantino, A. (2016). Application of microbially induced calcite precipitation in erosion mitigation and stabilisation of sandy soil foreshore slopes: A preliminary investigation. *Engineering Geology, 201*, 96–105. https://doi.org/10.1016/J.ENGGEO.2015.12.027

Sang, G., Lunn, R. J., El Mountassir, G., & Minto, J. M. (2023a). Meter-scale MICP improvement of medium graded very gravelly sands: Lab measurement, transport modelling, mechanical and microstructural analysis. *Engineering Geology, 324*, Article 107275. https://doi.org/10.1016/j.enggeo.2023.107275

Sang, G., Lunn, R. J., El Mountassir, G., & Minto, J. M. (2023b). Transport and fate of ureolytic Sporosarcina pasteurii in saturated sand columns: Experiments and modelling. *Transport in Porous Media, 149*, 599–624. https://doi.org/10.1007/s11242-023-01973-x

Sang, G., Lunn, R. J., El Mountassir, G., Minto, J. M., McLachlan, E., Bradley, D., & Henderson, K. (2024). Improving non-uniform gravelly sand using microbially induced carbonate precipitation: An outdoor cubic-meter scale trial by engineering contractors. *Engineering Geology*Article 107791. https://doi.org/10.1016/J.ENGGEO.2024.107791

Sharma, M., Satyam, N., & Reddy, K. R. (2022). Large-scale spatial characterization and liquefaction resistance of sand by hybrid bacteria induced biocementation. *Engineering Geology, 302*, Article 106635. https://doi.org/10.1016/j.enggeo.2022.106635

Song, C., Wang, C., Elsworth, D., & Zhi, S. (2022). Compressive strength of MICP-treated silica sand with different particle morphologies and gradings. *Geomicrobiology Journal, 39*, 148–154.

Stocks-Fischer, S., Galinat, J. K., & Bang, S. S. (1999). Microbiological precipitation of CaCO3. *Soil Biology and Biochemistry, 31*, 1563–1571. https://doi.org/10.1016/S0038-0717(99)00082-6

Terzis, D., Laloui, L., Dornberger, S., & Harran, R. (2020). A full-scale application of slope stabilization via calcite bio-mineralization followed by long-term GIS surveillance, in: *Geo-congress 2020* (pp. 65–73). Reston, VA: American Society of Civil Engineers.

Terzis, D., & Laloui, L. (2018). 3-D micro-architecture and mechanical response of soil cemented via microbial-induced calcite precipitation. *Scientific Reports, 8*, 1–11. https://doi.org/10.1038/s41598-018-19895-w

van Paassen, L.A. (2011). Bio-mediated ground improvement: From laboratory experiment to pilot applications. In *Proceedings of geo-frontiers; Advances in geotechnical engineering*.

van Paassen, L. A., Ghose, R., Linden, van der, T. J. M., Star, van der, W. R. L., Loosdrecht, & van, M. C. M. (2010). Quantifying biomediated ground improvement by ureolysis: Large-scale Biogrout experiment. *Journal of Geotechnical and Geoenvironmental Engineering, 136*, 1721–1728. https://doi.org/10.1061/(ASCE)GT.1943-5606.0000382

Whiffin, V. S., van Paassen, L. A., & Harkes, M. P. (2007). Microbial carbonate precipitation as a soil improvement technique. *Geomicrobiology Journal, 24*, 417–423. https://doi.org/10.1080/01490450701436505

Wu, H., Wu, W., Liang, W., Dai, F., Liu, H., & Xiao, Y. (2023). 3D DEM modeling of biocemented sand with fines as cementing agents. *International Journal for Numerical and Analytical Methods in Geomechanics, 47*, 212–240. https://doi.org/10.1002/NAG.3466

Wu, S., Li, B., & Chu, J. (2020). Large-scale model tests of biogrouting for sand and rock. Proceedings of the institution of civil engineers-ground improvement. https://doi.org/10.1680/JGRIM.18.00074.

Xiao, Y., Ma, G., Wu, H., Lu, H., & Zaman, M. (2022). Rainfall-induced erosion of biocemented graded slopes. *International Journal of Geomechanics, 22*, 4021256.

Xiao, Y., Stuedlein, A. W., Ran, J., Evans, T. M., Cheng, L., Liu, H., Paassen, L. A. van, & Chu, J. (2019a). Effect of particle shape on strength and stiffness of biocemented glass beads. *Journal of Geotechnical and Geoenvironmental Engineering, 145*, Article 06019016. https://doi.org/10.1061/(ASCE)GT.1943-5606.0002165

Xiao, Y., Yuan, Z., Lin, J., Ran, J., Dai, B., Chu, J., & Liu, H. (2019b). Effect of particle shape of glass beads on the strength and deformation of cemented sands. *Acta Geotechnica, 14*, 2123–2131. https://doi.org/10.1007/S11440-019-00830-W/FIGURES/8

Xiao, Y., Zhao, C., Sun, Y., Wang, S., Wu, H., Chen, H., & Liu, H. (2021). Compression behavior of MICP-treated sand with various gradations. *Acta Geotechnica, 16*, 1391–1400. https://doi.org/10.1007/S11440-020-01116-2/FIGURES/7

Zamani, A., Xiao, P., Baumer, T., Carey, T. J., Sawyer, B., & DeJong, J. T. (2021). Mitigation of liquefaction triggering and foundation settlement by MICP treatment. *Journal of Geotechnical and Geoenvironmental Engineering, 147*, Article 04021099. https://doi.org/10.1061/(ASCE)GT.1943-5606.0002596

Zeng, C., Veenis, Y., Hall, C. A., Young, E. S., van der Star, W. R. L., Zheng, J., & van Paassen, L. A. (2021). Experimental and numerical analysis of a field trial application of microbially induced calcite precipitation for ground stabilization. *Journal of Geotechnical and Geoenvironmental Engineering, 147*, Article 05021003. https://doi.org/10.1061/(ASCE)GT.1943-5606.0002545

Zhang, J., Yin, Y., Shi, W., Bian, H., Shi, L., Wu, L., Han, Z., Zheng, J., & He, X. (2023). Strength and uniformity of EICP-treated sand under multi-factor coupling effects. *Biogeotechnics, 1*, Article 100007. https://doi.org/10.1016/J.BGTECH.2023.100007